A climate-dependent spatial epidemiological model for the transmission risk of West Nile virus at local scale

Anastasia Angelou [a], Ioannis Kioutsioukis [a,*], Nikolaos I. Stilianakis [b,c]

[a] Department of Physics, University of Patras, Greece
[b] European Commission, Joint Research Centre (JRC), Ispra, Italy
[c] Department of Biometry and Epidemiology, University of Erlangen-Nuremberg, Erlangen, Germany

ABSTRACT

In this study, initial elements of a modelling framework aimed to become a spatial forecasting model for the transmission risk of West Nile virus (WNV) are presented. The model describes the dynamics of a WNV epidemic in population health states of mosquitoes, birds and humans and was applied to the case of Greece for the period 2010–2019. Calibration was performed with the available epidemiological data from the Hellenic Centre for Disease Control and Prevention and the environmental data from the European Union's earth observation program, Copernicus. Numerical results of the model for each municipality were evaluated against observations. Specifically, the occurrence of WNV, the number of infected humans and the week of incidence predicted from the model were compared to the corresponding numbers from observations. The results suggest that dynamic downscaling of a climate-dependent epidemiological model is feasible down-to roughly 80km^2. This below nomenclature of territorial units for statistics (NUTS) 3 level represents the municipalities being the lowest level of administrative units, able to cope with WNV and take actions. The average detection probability in hindcast mode was 72%, improving strongly as the number of infected humans increased. Using the developed model, we were also able to show the fundamental importance of the May temperatures in shaping the WNV dynamics. The modeling framework couples epidemiological and environmental dynamical variables with surveillance data producing risk maps downscaled at a local level. The approach can be expanded to provide targeted early warning probabilistic forecasts that can be used to inform public health policy decision making.

1. Introduction

According to World Health Organization (WHO) estimates vector-borne diseases are a global health threat and cause more than 700,000 deaths globally each year [1] with substantial economic and social impacts. Environmental, including climate, phenomena contribute to the establishment of the necessary conditions for vector-borne diseases to thrive. Factors such as temperature and precipitation affect survival and reproduction rates of infectious diseases vectors and pathogens [2]. Climatic factors influence vector-borne disease ecology changing the geographic and seasonal distribution, and the intensity of vector-borne pathogen transmission, hence modifying the probability of epidemics [3].

West Nile virus (WNV) is the causative pathogen for West Nile Fever (WNF) and West Nile neuro-invasive disease (WNND) in humans. WNV belongs to the *flavivirus* genus and it is a neurotropic mosquito-borne virus [4]. The virus was first isolated in the West Nile district of Uganda in 1937 [5]. The transmission and geographic distribution of WNV is associated with the presence of both the avian host and mosquito vector, which is affected by environmental and socio-economic conditions. These conditions can influence viral persistence and the dynamics of outbreaks [6]. The virus is maintained in nature in a mosquito-bird-mosquito transmission cycle. Mosquitoes of the genus *Culex* are generally considered the principal vectors of WNV, especially *Culex Pipiens* [7–9]. Wild birds are the predominant reservoir hosts of WNV [10]. Human infection is most often the result of bites from infected mosquitoes. Mosquitoes become infected when they bite infected birds and the virus circulates in their blood for a few days. Bites of infected mosquitoes may inject the virus into humans and animals, in some of which the virus can cause severe illness. They are "dead-end" hosts, so they become infected, but they do not develop sufficient high viremia to pass the virus on to other biting mosquitoes [11]. The incubation period

is 2–14 days. WNV has the potential to adapt into new environmental conditions [12]. About 80% of the infections in humans are asymptomatic, while about 20% are present as a mild illness (characterized by fever, headache, chills, excessive sweating, fatigue, muscle pain, malaise, arthralgia, nausea, anorexia, diarrhea, vomiting, rash, and swollen lymph nodes) known as WNF. In less than 1% of the infections in humans a WNND, is manifested with symptoms of the central nervous system mainly encephalitis, but also meningitis, meningoencephalitis, or acute flaccid paralysis. The fatality rate of WNND cases is approximately 10%. Population vulnerable groups at risk are the elderly and persons with an underlying disease or with immunosuppression. A significant number of patients develop long-term or permanent impairments (like depression, fatigue, cognitive deficits, movement disorders or paralysis) [13,14]. Currently no human vaccine is available. Therefore, the principal way to prevent or reduce the infection burden in people is by educating people about the measures they can take to reduce exposure to the virus and raising awareness of the risk factors [11].

The role climatic factors may play in the epidemiology of WNV infections in humans is indicated in associative studies pointing to the relevance of taking them into consideration when evaluating the risk of pathogen transmission and disease spread [15]. Temperature, precipitation, relative humidity, soil water content and wind speed have been associated with WNV prevalence [16–19]. However, quantitative assessments with partially contradicting results, and the complex zoonotic transmission cycle make the establishment of evidence and causative attribution a major challenge [20,21].

Culex mosquitoes typically breed underground in the foul water standing in city drains and catch basins [22]. During a drought, those pools become richer in the rotting organic material that the mosquitoes need to prosper. Drought can also lead to a decline in the number of mosquito predators and it may encourage birds to congregate around water sites, where the virus can circulate easily [23–26]. However, heavy rainfall can flush larval habitats and reduce mosquito abundance [27,28]. Increasing ambient temperature results in increasing rate of development and abundance of mosquito populations and decreasing extrinsic incubation period [29–32]. These factors increase the levels of infection in birds and mosquitoes living close to human settlements [33]. In addition, weather may affect the bird migration. It has been shown that short-term variation in environmental conditions might cause a change in the bird migration route [34]. To adapt to climate variability, the long-distance migratory birds choose to stop earlier when the weather conditions are not favorable, while the short-distance migratory birds decide not to migrate [12].

Two striking events have characterized the global epidemiology of WNV over the last decades: the outbreak in Romania in 1996 with 393 human cases [35] and the introduction of the virus into the Americas in late summer 1999 [36]. Over the last decades there have been multiple outbreaks in humans and equids in eastern and southern Europe where a substantial increase in WNV infections among humans was observed in particular during the period 2010–2018 [37,38]. In Greece, two major outbreaks of the virus occurred in the decade 2010–2019. In 2010 (year of first detection), a WNV outbreak caused a total of 262 human cases, 197 of these with WNND and 35 deaths. The majority of human cases occurred in the Region of Central Macedonia in Northern Greece. In 2018, 316 people were infected, 243 developed WNND and 50 died. Most of human cases were observed in Central Macedonia and Attica Region [14].

A wide range of both predictors and modeling approaches have been described in the literature for early detection, identification of spatial patterns and forecasting vector-borne diseases such as WNV using diverse techniques and relevant data including geospatial surveillance such as earth observation data [39,40]. Several mathematical models of WNV transmission have been developed to predict the transmission dynamics of the virus. Most of them are process-based models elaborating predominantly on the temporal and spatial spread of WNV

transmission in the mosquito-bird population zoonotic cycle [41–47]. Seasonality effects such as seasonal variation or the effects of specific climatic factors like temperature have also been addressed [17,48–50]. Some approaches indicate that epidemiological models forced by climatic factors such as temperature can improve forecast accuracy including the estimation of the highest risk of infection in humans during the transmission seasonal periods [51,52]. Specific aspects of overwintering of bird communities could sustain WNV persistence [53]. Laperriere et al. [54] focused on seasonal cycles of WNV cases under consideration of environmental temperature as a guide to the extrinsic incubation period of mosquitoes that extends a model originally developed by Rubel et al. [55]. Kioutsioukis and Stilianakis [56] explored the associations between weather and WNV using a previously developed epidemiological model that describes the transmission dynamics of WNV during the transmission cycle. The original model relied on a series of daily temperature data estimated on the basis of monthly averages of temperature [54,55]. Kioutsioukis and Stilianakis [56] extend the model to build upon daily temperature and precipitation time series, where daily fluctuations are filtered out, both known to influence the transmission of the virus. In addition, they test the influence of different functions that parameterize the mortality of mosquitos. The functions differ in the temperature range, thus providing the necessary adjustment of the mathematical model to climatically different geographical areas [56].

In this study, we describe initial steps of a spatial forecasting model (MIMESIS: spatial dynaMIcal Model for wESt nIle viruS) for the transmission risk of WNV to humans and the investigation of its climatic sensitivity. We employ an epidemiological model that describes the transmission cycle of the WNV and couple it with the climatic factors. We develop the proper scaling of model and data and use retrospective data and simulations to create maps of human cases at the level of municipality such as maps with indicators of model goodness of fit and predictive power. These indicators could be for instance probability of detection, false positive and false negative incidences. As a case study, we used all municipalities of Greece for the period 2010–2019 and calibrated the model with the available epidemiological data from the Hellenic Centre for Disease Control and Prevention (HCDCP) and the environmental data from the European Union's earth observation program, Copernicus. We validated the model with observations from each municipality comparing predicted versus observed cases. We could uncover associations between emergence of human case and climatic conditions that underline the role of seasonality in WNV transmission.

2. Data and methodology

2.1. Investigation area and data

The study area was Greece. According to the 2011 census [57], the country has a population of 10,816,286 inhabitants, and it covers an area of 132,028.848 km^2. The country is divided into seven decentralized administrations, 13 regions and 325 municipalities.

Before we fed the modelling system with the appropriate environmental data, we created a database with essential epidemiological and environmental data such as latitude, longitude, human population, area [57], wild bird populations [58], number of infected humans and week of first incidence in each municipality [59].

2.1.1. Population data

Our study was conducted at the local (municipal) level, which is not covered by the spatially broader nomenclature of territorial units for statistics (NUTS) levels. Data on the local administrative division of the country, the permanent population of the residents and the area of each municipality were obtained from the Hellenic Statistical Authority (HSA). Latitude and longitude of each municipality were taken from Google maps.

Data on the wild bird populations (namely *Pica pica, Corvus cornix,*

Streptopelia turtur, Turdus philomelos, Anas platyrhynchos, Turdus merula, Cuculus canorus, Passer domesticus, Hirundo rustica) were obtained from the European Breeding Birds Atlas (EBBA) of the European Bird Census Board (EBCC) [58]. These species are competent for WNV transmission in the study area and are considered the most important avian reservoirs for the virus. The EBBA grid cells have 0.5^o x 0.5^o resolution. In order to find the total population of bird species for all municipalities in Greece, the size of the cell and the area of each municipality were taken into account.

2.1.2. Epidemiological data

Data of the epidemiological activity of WNF and WNND in humans in Greece the period 2010–2019 were obtained from the HCDCP. It is worth mentioning that a large part of WNV infections in humans shows either a few non-specific clinical symptoms or run as subclinical infections (asymptomatics) and are unobserved. Thus, notification of human cases is usually limited to those cases of infected individuals who seek medical advice or severe cases that need hospitalization. The epidemiology of WNV in humans is based on these cases and the real number of WNV human cases is unknown. The undocumented fraction of infections has been estimated to surpass the reported number of cases by two orders of magnitude [59].

2.1.3. Environmental data

Air temperature and precipitation were considered as critical climate factors and were embedded in the modeling approach. Temperature data from Greece were obtained from ERA 5 (fifth major global reanalysis from the European Centre for Medium-Range Weather Forecast) (ECMWF) and referred to the period 1980 to 2019 for four hours each day. From these data, the daily mean, maximum and minimum temperature were estimated. To eliminate fluctuations, we applied a filter to the temperature time series. Daily precipitation data for the same area and period were also obtained from ERA 5 since there are indications that the development of pools suitable for *Culex* larvae to deposit eggs optimally require moderate precipitation [60].

2.2. MIMESIS description

MIMESIS is based on the model proposed by Rubel et al. [55] and extended by Leperriere et al. [54] and Kioutsioukis and Stilianakis [56]. Kioutsioukis and Stilianakis [56] developed a regional level model for the Regional Unit of Thessaloniki in North Greece and the air temperature as the climatic factor with which the model is powered. MIMESIS is a downscaled version of this model for all municipalities of Greece, which is forced by air temperature and precipitation. The compartmental model simulates the seasonal lifecycles of birds, mosquitoes and the inter-specific WNV infection cycle between birds and mosquitoes. The state "recovered" denotes those hosts that do not further contribute to the infection process and this state is further divided into recovered and dead birds and humans. Thus, MIMESIS has 14 compartments (i.e. health states); four states for the vector mosquito (larvae L_M, susceptible S_M, exposed E_M and infectious I_M); five states for amplifying host, birds (susceptible S_B, exposed E_B, infectious I_B, recovered R_B and dead D_B), and five states for the dead-end host humans (susceptible S_H, exposed E_H, infectious I_H, recovered R_H and dead D_H). The full system of equations for all compartments is provided in Appendix A.

2.2.1. Parameter definition

Details on MIMESIS parameters can be found in the Appendix B.

2.2.2. Fixed parameters

Parameters that had a fixed value included the probability of transmitting the virus from a mosquito to a bird (p_M), the mortality rate of birds (m_B), the probability of transmitting the virus from a bird to a mosquito (p_B), the removal rate of birds (a_B), extrinsic-incubation period of birds (γ_B), the fraction birds dying due to the infection (ν_B), the

mosquito-to-bird ratio (φ_B), the birth rate of humans (b_H), the mortality rate of humans (m_H), the recovery rate of humans (a_H), the transition rate from exposed (infected but not infectious) to infected and infectious of humans (γ_H), the reproduction rate of humans (r_H) and the fraction humans dying due to infection (ν_H).

2.2.3. Parameters with geographical dependence

The carrying capacity of birds (K_B) had a different value for each municipality. Specifically, from the data obtained from the EBCC the population density of birds was determined. This density (birds/km^2) was multiplied by the area of each municipality (km^2) to estimate a carrying capacity adjusted to local scale. Spatially dependent parameters also included the initial population of infectious mosquitoes ($I_{M,0}$), the mosquito-to-human ratio (φ_H), the population of susceptible mosquitoes ($S_{M,0}$) and the population of susceptible humans ($S_{H,0}$).

2.2.4. Biological parameters with seasonal dependence

The birth (hatch) rate of larvae (b_L) and the birth (emergence) rate of mosquitoes (b_M) had a temperature-dependent value, like the mortality rate of larvae (m_L), the mortality rate of mosquitoes (m_M), the biting rate of mosquitoes (k) and the extrinsic-incubation period of mosquitoes (γ_M). Birth rate of birds (b_B) was simulated as a function of the Julian day, while the fraction of active mosquitoes (δ_M) was a fraction of the daytime length. The carrying capacity of mosquitoes (K_M) of each municipality depends on the carrying capacity of birds (K_B), the mosquito-to-bird ratio (φ_B) and the precipitation according to a specific formula [56].

2.2.5. Initialization and calibration

MIMESIS was solved numerically in MATLAB R2019b with a time step of one day. It was forced by the ambient temperature via the temperature-dependent mosquito and bird parameters, and the precipitation via the carrying capacity of mosquitoes. Before we fed the system with temperature data, we applied a Kolmogorov-Zurbenko [61] filter to smooth temperature time series.

Our simulation started in winter (January) and the initial population of mosquito larvae ($L_{M,0}$) was set to zero. The initial population of susceptible mosquitoes ($S_{M,0}$) was equal to the number of hibernating mosquitoes ($N_{M,min}$). This population was estimated proportionally based on data from the Regional Unit of Thessaloniki in North Greece [56]. The initial number of susceptible people to the virus ($S_{H,0}$) was different for each municipality and was equal to the population of people living in this municipality ($N_{H,0}$). The initial number of susceptible birds ($S_{B,0}$) was equal to the carrying capacity of birds (K_B). The values of the initial population of infectious mosquitoes ($I_{M,0}$) and the mosquito-to-human ratio (φ_H) were estimated after the model calibration. The calibration of the model was done by minimizing the Root-Mean-Square Error (RMSE) between observed and modeled annual human cases. Specifically, tests were performed for values of the initial population of infectious mosquitoes ($I_{M,0}$) between 1 and 201 with a step of 20 and for values of the logarithm of the mosquito-to-human ratio (φ_H) from −5 to −1 with a step of 1. Thus, the appropriate pair of the initial population of infectious mosquitoes ($I_{M,0}$) and the mosquito-to-human ratio (φ_H) values was found; we assumed $I_{M,0}$ to be a function of municipality and year while φ_H only depends on municipality. The weak constraint on φ_H was imposed to avoid overfitting the model, increasing its potential forecasting skill at a next stage. The initial values of exposed mosquitoes, birds and humans ($E_{M,0}$, $E_{B,0}$, $E_{H,0}$), of infected birds and humans ($I_{B,0}$, $I_{H,0}$), of recovered birds and humans ($R_{B,0}$, $R_{H,0}$), as well as the initial values of dead birds and humans ($D_{B,0}$, $D_{H,0}$) were set to zero.

2.3. Statistical measures for model verification

For the purposes of model verification, we define as a "WNV event" the case where at least one human infection is recorded at a municipality

during a specific year. The validation of the model's ability to correctly identify WNV events spatially and temporally is performed with the aid of hits (hereafter a; obs/mod T/T: number of municipalities where WNV events were both observed and simulated at a specific year), the false alarms (hereafter b; obs/mod F/T: number of municipalities where WNV events were simulated at a specific year but they were not observed), the misses (hereafter c; obs/mod T/F: number of municipalities where WNV events were not simulated at a specific year but they were observed) and the correct negatives (hereafter d; obs/mod F/F: number of municipalities where WNV events were not observed nor simulated at a specific year). The four indices a, b, c, d allow the computation of the following statistical indicators for the WNV events:

- Hit Rate or Probability of Detection (POD), Range [0, 1], Best score 1

$$POD = \frac{a}{a + c}$$

- Miss Rate (MIS), Range [0, 1], Best score 0

$$MIS = 1 - H = \frac{c}{a + c}$$

- False-alarm rate (FAR), Range [0, 1], Best score 0

$$FAR = \frac{b}{a + b}$$

- Threat Score or Critical Success Index (CSI), Range [0, 1], Best score 1

$$TS = CSI = \frac{a}{a + b + c}$$

Apart from the validation of categorical variables (WNV events), we also quantify the model's ability to replicate, at each municipality, the observed number of annual human infections as well as the observed week of the first human infection. For those assessments we employ qualitative plots (scatterplots, residual plots) as well as quantitative measures for the goodness of fit, including the mean bias (MB), the root mean squared error (RMSE) and the coefficient of determination (R^2).

3. Results

The geographical distribution of the reported WNV human cases is given in Fig. 1. The 325 municipalities are colored according to the number of years in the decade 2010–2019 where at least one human case appeared (i.e. number of "WNV events" in the decade). One hundred seventy-three (173) municipalities were WNV free (Fig. 1 in white). In the remaining one hundred fifty-two (152) municipalities, WNV human cases observed from one up to six years. Specifically, in 62 out of 152 municipalities (41%) human cases were observed only in one year during the decade while in 44 municipalities (29%) human cases were found in two years. The municipalities where WNV incidences appeared in three or four years of the decade represent the 26% of the infected areas (40 out of 152). Last, at 4% of the infected municipalities (6 out of 152), WNV cases were reported in five or six years of the decade.

Following the development of the necessary spatial input databases, optimal values for two parameters of MIMESIS were estimated. The initial population of infectious mosquitoes ($I_{M,0}$) has spatial and temporal (annual) dependence while the mosquito-to-human ratio (φ_H) exhibits only geographical dependence. This design also allows the potential use of MIMESIS in forecast fashion, provided we can only infer $I_{M,0}$ through an independent procedure.

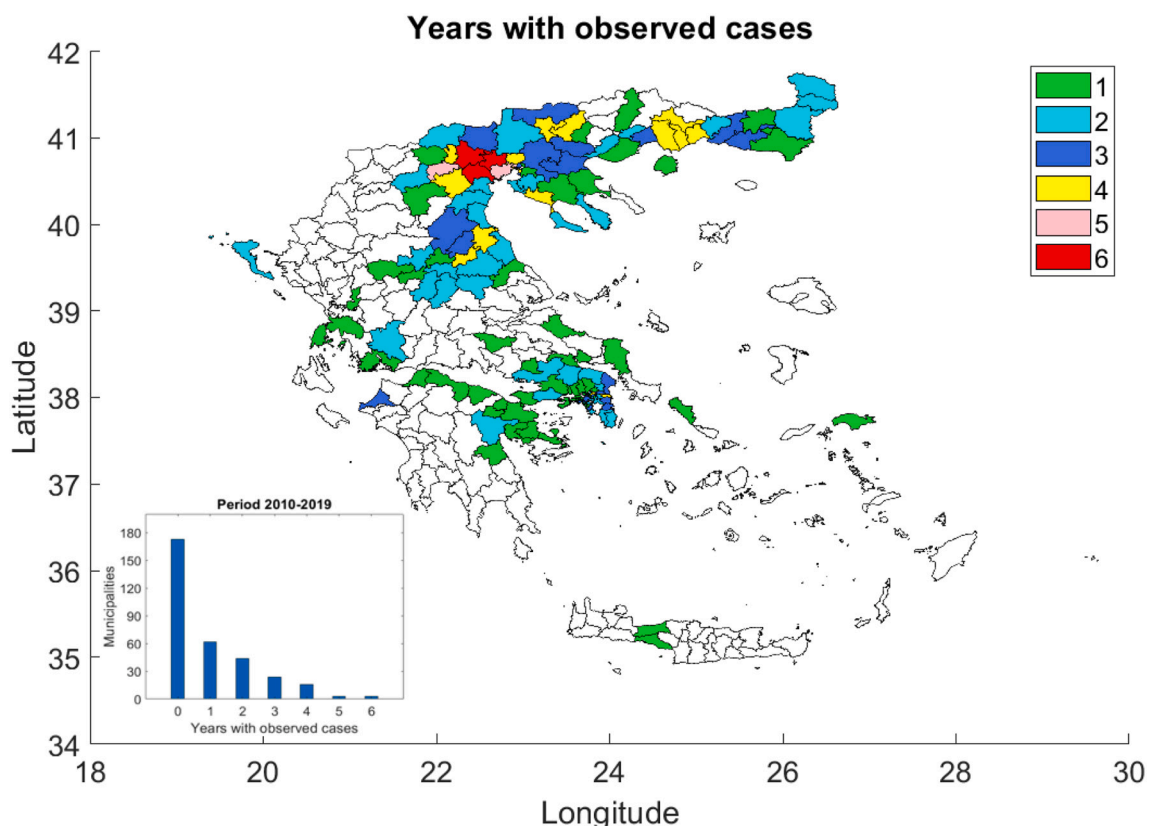In section 3.1 we present the model evaluation. Case studies are

Fig. 1. Geographical distribution of the number of years per municipality with at least one reported WNV human case over the decade 2010–2019.

demonstrated in section 3.2. In section 3.3, MIMESIS was used in a climatic sensitivity study.

3.1. Model evaluation (2010–2019)

First, we investigated in 3.1.1 the skill of MIMESIS to correctly discriminate WNV events. Then, in 3.1.2 we quantified the MIMESIS skill with respect to the annual number of human cases and the timing of the 1st human case.

3.1.1. Occurrence of WNV events

3.1.1.1. Spatial analysis. We investigated the capability of MIMESIS to capture the spatial occurrence of WNV events in the decade 2010–2019. The analysis relies on the four indices presented in section 2.3. Out of 3250 potential WNV events over the decade (325 municipalities times 10 years), WNV events occurred 319 times (sum of the annual number of municipalities where human cases occurred, in the decade). MIMESIS identified correctly the 229 cases (hits, index a, section 2.3) and generated false alarm at 109 cases (index b, section 2.3). All (2822) correct negatives (index d, section 2.3) were excluded from the subsequent analysis to avoid deceptively good validation statistics.

Each index (POD, FAR, MIS, CSI) takes values between 0 and 1. We split this range into five equally sized zones with 0.2 extent each and calculate the number of municipalities within each zone for every index (Table 1). Fig. 2 shows the geographical distribution of the results shown in Table 1. The probability of detection exceeds 0.8 in 88 out of the 152 municipalities. This is a promising result, especially when combined with the low probability (<20%) for false alarms or misses at 84 and 89 municipalities respectively. Using the CSI, we found 62 municipalities exceeding 0.8 of CSI, while overall 62.5% (95/152) of the municipalities have CSI larger than 0.5. As expected, the CSI was lower than the corresponding POD as CSI utilizes not only hits but also incorporates the failures due to misses and false alarms. At the other tail of the indices, we found 36 municipalities with low POD (and high MIS) rate. An error analysis follows in the next paragraphs.

In Fig. 3a the 152 municipalities which faced WNV events are clustered, according to their area, into ten equal quantiles. The lower 10% of the municipalities have area smaller than $6.5km^2$, the next 10% have area between $6.5km^2$ and $16km^2$, and the next 10% have area between $16km^2$ and $83km^2$. A similar clustering for the 36 municipalities with POD<0.2 shows that 39% (55%) of them occupy areas smaller than 16 km^2 (83 km^2), rather than 20% (30%). Therefore, 20 out of the 36 municipalities with low POD belong to municipalities with area smaller than $83km^2$; the majority (14 of 20) occupy area smaller than 16 km^2 and belonged to densely populated urban units in the area of Athens and Thessaloniki, where roughly half population of the country resides. The remaining 16, as could be identified from Figs. 1 and 2, belonged to municipalities where WNV events occurred only once in the last decade.

The median POD and CSI, at each of the ten equally sized area zones identified in Fig. 3a, is shown in Fig. 3b. The median POD equals one for municipalities with area larger than 16 km^2. CSI values initially oscillate, exceed 0.5 for municipalities with area larger than 83 km^2 and

Table 1
The examined indices POD, FAR, MIS and CSI decomposed into five accuracy zones, with the number of municipalities at each band.

	Number of Municipalities			
	POD	FAR	MIS	CSI
[0% … 20%]	36	84	89	38
(20% … 40%]	4	8	14	18
(40% … 60%]	11	11	9	22
(60% … 80%]	13	11	4	12
(80% … 100%]	88	2	36	62
SUM	**152**	**116**	**152**	**152**

reach 1 when the area exceeds 413 km^2. Those results indicate that the lowest downscaling threshold is approximately 83 km^2.

3.1.1.2. Temporal analysis. To complement the spatial analysis, we investigated the capability of MIMESIS to capture the temporal occurrence of WNV events in the decade 2010–2019. The multi-annual evolution of the indices is shown in Table 2. The spatially aggregated POD was 0.72 over the decade. The model correctly identified the location and year for the 72% of the observed human cases (and missed 28% of them). Annually, POD varied between 0.57 (2014) and 0.89 (2010). The aggregated decadal FAR was 0.32, ranging from 0.08 (2019) to 1 (2015–2016). The FAR index reached particularly high values (0.67–1) in the period 2014–2017, when a WNV hiatus occurred. The combined effect of hits, misses and false alarms expressed through the CSI index showed an average value of 0.54. CSI varied between 0.48 and 0.73 outside the hiatus period and took low values (0–0.27) during the hiatus. Those results imply a relation between the indices and the number of IH (or municipalities where human cases occurred), more profound for FAR and CSI. Indeed, the R^2 in the linear fit between the annual indices and the annual number of infected municipalities is 0.76 in the case of CSI and 0.83 for FAR, both being significant at the 5% significance level (not shown). Detection probability and false alarms improved as WNV spread increase.

3.1.2. Severity and timing of WNV events

3.1.2.1. Number of infected humans

3.1.2.1.1. Analysis at the decade. Simulation results for the decade, i.e. the scatter plot of the total number of observed and modelled infected human cases at each municipality for the period 2010–2019 are shown in Fig. 4a. The R^2 is 0.88 indicating that MIMESIS accounted for 88% of the spatial variability in decadal scale. Most of the municipalities in the scatter plot are distributed in a narrow band around the main diagonal. Indeed, within the ±25% bounds (inner black dotted lines) lie 66 of the 152 municipalities (correct negatives excluded) while within ±50% error there are in total 92 municipalities. Between the ±50% and ± 99% error there are another 21 municipalities. Thirty-six municipalities have 100% error (i.e. $IH_{MOD} = 0$, corresponding principally to urban areas and municipalities facing only one WNV event, as discussed in 3.1.1), and last 3 municipalities have fractional error over 100%. The number of observed and modelled infected humans per municipality, split into six zones according to the observed number of human infections, is shown in Table 3. It is evident that the general underestimation tendency is homogeneous across the bins, supporting the hypothesis that there is no structural error in the model. The above statements are evident in Fig. 4c-4d, which is the spatial version of Fig. 4a and Table 3. The annual disaggregation of Fig. 4b is available in the supplementary data (Fig. S1-Fig. S11).

3.1.2.1.2. Analysis at annual scale. The number of infected humans (amplitude of event) is analyzed together with the occurrence of a WNV event. Specifically, we excluded the 2822 correct negatives and analyzed the error in the remaining 428 cases (hits + misses + false alarms). The distribution of 229 hits included a range of modelled infected humans between 1 and 26, with most frequent (Table 4) being one human case (104 times), two cases (35 times) and three cases (23 times). Regarding the 109 false alarms, the modelled number of human cases was either 1 (104 times) or 2 (5 times). For the 90 misses, the observed number of human cases was principally 1 (72 times), followed by 2 (11 times), 3 (4 times), 5 (2 times) and 7 (1 time). Combined all together, it was evident that if one human case was simulated, the actual probability of occurrence was 50% (104 hits and 104 false alarms). At the same time, at 80% of the misses (72 out of 90) the observed number of infected humans was one. Therefore, when the modelled number of human cases was larger than one, there were no false alarms, i.e. the event forecast uncertainty diminished.
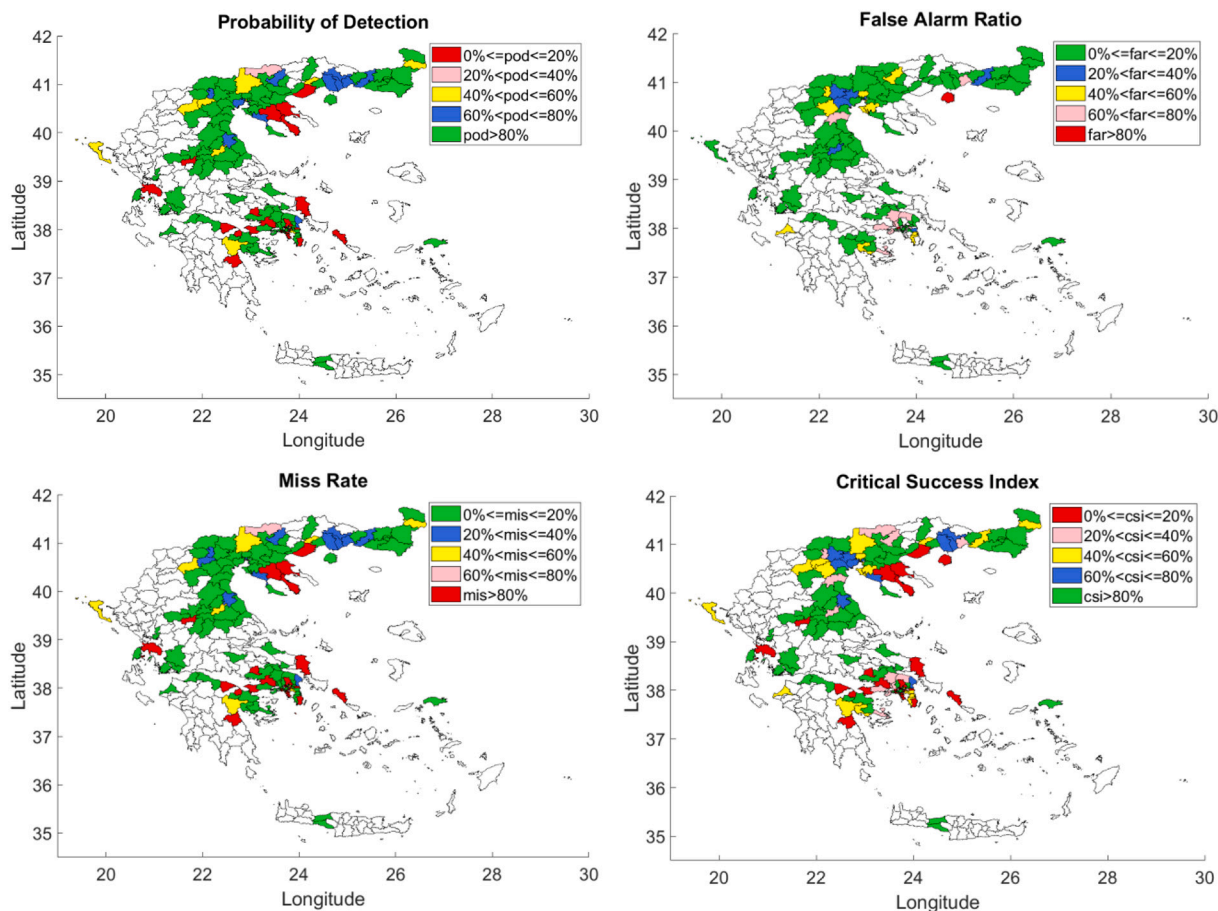
Fig. 2. Maps of categorical measures/scores split into five accuracy zones: Probability Detection (top left), False alarm Ratio (top right), Miss Rate (bottom left), Critical Success Index (bottom right).
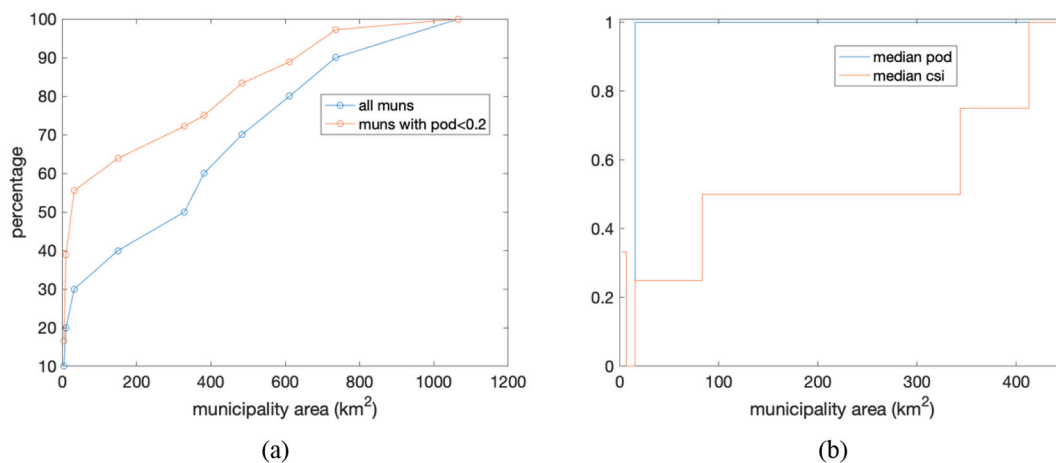

Fig. 3. (a) The cumulative percentage of the municipalities according to their area split into ten equally sized zones (blue), and the percentage of municipalities within each zone with POD<0.2 (red) (b) The median POD (blue) and CSI (red) at each equally sized area zone. (For interpretation of the references to colour in this figure legend, the reader is referred to the web version of this article.)

Fig. 4b shows the bias of each case versus the number of infected humans, where hits (open circles) are distinguished from misses (asterisks) and false alarms (filled circles). The mean bias (MB) is −0.7 (underestimation) and the standard deviation (SD) of the residuals is 2.7. Within the limits [MB-2SD, MB + 2SD] lied 96% of the data, supporting the hypothesis the residuals were normally distributed.

The multiannual variability of the total number of predicted and observed human cases at each year is presented in Fig. 4e. During the decade 2010–2019, four extreme years occurred; 2015 and 2016 without any WNV human case and, 2010 and 2018 with a regional outbreak. The model simulations followed the year-to-year trend in the annual number of human cases. This occurred across the whole range of annual human cases, indicating the proper calibration of the model. At the same time, the figure shows that MIMESIS has the tendency to

Table 2
Temporal evolution of the annual score in the examined indices POD, FAR, MIS and CSI.

Year	Infected municipalities	$\sum IH_{OBS}$	POD	FAR	MIS	CSI
2010	38 (12%)	262	0.89	0.26	0.11	0.68
2011	46 (14%)	100	0.63	0.09	0.37	0.59
2012	42 (13%)	157	0.60	0.32	0.40	0.46
2013	35 (11%)	85	0.74	0.42	0.26	0.48
2014	7 (2%)	15	0.57	0.67	0.43	0.27
2015	0	0	–	1	–	0
2016	0	0	–	1	–	0
2017	10 (3%)	48	0.7	0.72	0.30	0.25
2018	85 (26%)	306	0.71	0.10	0.29	0.65
2019	56 (17%)	223	0.79	0.08	0.21	0.73
2010–19	319 (10%)	1196	0.72	0.32	0.28	0.54

underestimate the high values of infected humans, as already seen in Fig. 4b.

The MB of the annual number of infected humans at each municipality, calculated over the 10 years and normalized with the range of IH at each municipality presents a normalized estimate of MB (NMB). A similar normalized index can be constructed from RMSE (NRMSE). The NMB vs NRMSE plot (soccer diagram) shows that the majority of models have normalized mean biases below 30% and mostly below 15% (Fig. 4f).

The main conclusions from the analysis of the simulated number of infected humans are:

- The interannual variability of WNV dynamics at local scale was captured. MIMESIS predicted lower number of infected humans across all years except during the hiatus period 2014–2017, when overestimation occurred.
- The most difficult situation to model was when there was only one human case annually per municipality. Above this threshold, the event simulation uncertainty diminishes.
- MIMESIS was unbiased at low incidences (IH < 5), exhibited small underestimation tendency at intermediate cases (5 < IH < 10) and larger underestimation at local outbreaks (IH > 10).

3.1.2.2. Week of 1st incidence. Next, we focus on the timing of the WNV incidences. The week of occurrence of the first human case for each municipality and year in 2010–2019 is presented in Fig. 5 by means of scatter plots between the model simulations and the official data. The week of the first incidences varies between 22 and 43 depending on the municipality and year. The corresponding modelled from MIMESIS range was 18–44. The municipalities are scattered around the diagonal, indicating an overall unbiased representation of the environmental and entomological parameterizations. Between the ±25% threshold lines we found the majority (85% - 91%) of the municipalities, with the rest indicating principally the false alarms (points on the y-axis) and the misses (points on the x-axis). The spatial version of Fig. 5 is available in the supplementary data (Fig. S12-Fig. S21).

3.2. Case studies

In this section we provide illustrative examples at selected municipalities where MIMESIS performed best and worst. For this purpose, municipalities were divided into three categories depending on the number of years where at least one human case was observed. Each category included the municipalities in which at least one human case was observed for 1–2, 3–4 and 5–6 years during the decade. At each category, the municipality with the minimum and maximum absolute mean bias $|sum(IH_{mod}) - sum(IH_{obs})|$ were selected to present the multiannual performance of the model.

At 106 municipalities in which at least one human case observed for one or two years, there were 32 municipalities where the absolute value

of the difference during the decade equals zero. Fig. 6a shows one such municipality, where the number of modelled infected humans equals the observed infected humans in two isolated years, 2011 and 2019. On the opposite side, there is one municipality where the absolute value of the difference during the decade equals 15. As can be seen in Fig. 6b, the model predicted one human case while 16 human cases were observed in 2012. MIMESIS correctly identified the event in the right year but missed its magnitude.

At 40 municipalities in which at least one human case was observed for three or four years, there were four municipalities where the absolute value of the difference equals zero. Fig. 6c shows one of these municipalities, where the number of modelled infected humans equals the observed infected humans in the three years 2014, 2018 and 2019. In contrast, there was one municipality where the absolute value of the difference during the decade equals 16. Fig. 6d shows that in this municipality there was high year-to-year variability. MIMESIS captures the occurrence in the outbreak year (2010) but not its magnitude, the model did very well in the other three years (2011, 2012, 2018) and demonstrated just a few false alarms at other four years.

Finally, from the six municipalities in which at least one human case was observed for five or six years, there were two municipalities where the absolute value of the difference during the decade equaled to two. One of these was presented in Fig. 6e. The bias was either zero or one in the outbreak years 2010 and 2018; however, the model did not capture the three cases in 2019. On the other side, there was one municipality in which the absolute value of the difference equaled to 26. Specifically, in this municipality the model correctly identified the years of occurrences and their magnitude, except for the outbreak year 2010 that penalized its performance.

The case studies demonstrated that overall, MIMESIS captures well the dynamics and the inter-annual variability of WNV.

3.3. Meteorological sensitivity

Following the calibration of the model over the decade 2010–2019, we investigate the sensitivity of the model output to the meteorological conditions, all other inputs kept at their optimal values. A total of 298 decadal simulations at each municipality were performed. They correspond to all possible combinations of 1 °C perturbations in the monthly temperatures of up to three months $\left(\left(\frac{12}{1} \right) + \left(\frac{12}{2} \right) + \left(\frac{12}{3} \right) \right)$. To avoid spurious results, we filtered out the simulations at municipalities without human cases over 2010–2019. At each of the 116 municipalities, we considered the most severe meteorological situation with respect to the total number of infected humans. Moreover, we filtered out the eighteen units that are climatologically neutral (the increase in IH was below 1). The results for the remaining 96 municipalities are presented in Table 5, where only 10 (out of the 298) combinations ultimately appear. The same table provides median estimates for (a) the meteorological impact, evaluated with the increase in the total number of human cases and (b) the local skill, evaluated with the CSI in the historical simulations. The main conclusions are:

- *Single month effect* (23 municipalities): at 22 of the total 96 municipalities (23%), the annual number of infected humans was found sensitive to the temperature anomaly in May, resulting in a median increase of 33% in the total number of cases. The corresponding municipalities had a median CSI of 1.
- *Bi-month effects* (20 municipalities): at 19 of the total 96 municipalities (20%), the annual number of infected humans was found sensitive to the temperature anomaly in April-May (7%) and May-June (13%), resulting in a median increase in the total number of cases of 25% and 39% respectively. In both cases, the corresponding municipalities had a median CSI of 1.
- *Tri-month effects* (53 municipalities): at 49 of the total 96 municipalities (51%), the annual number of infected humans was found
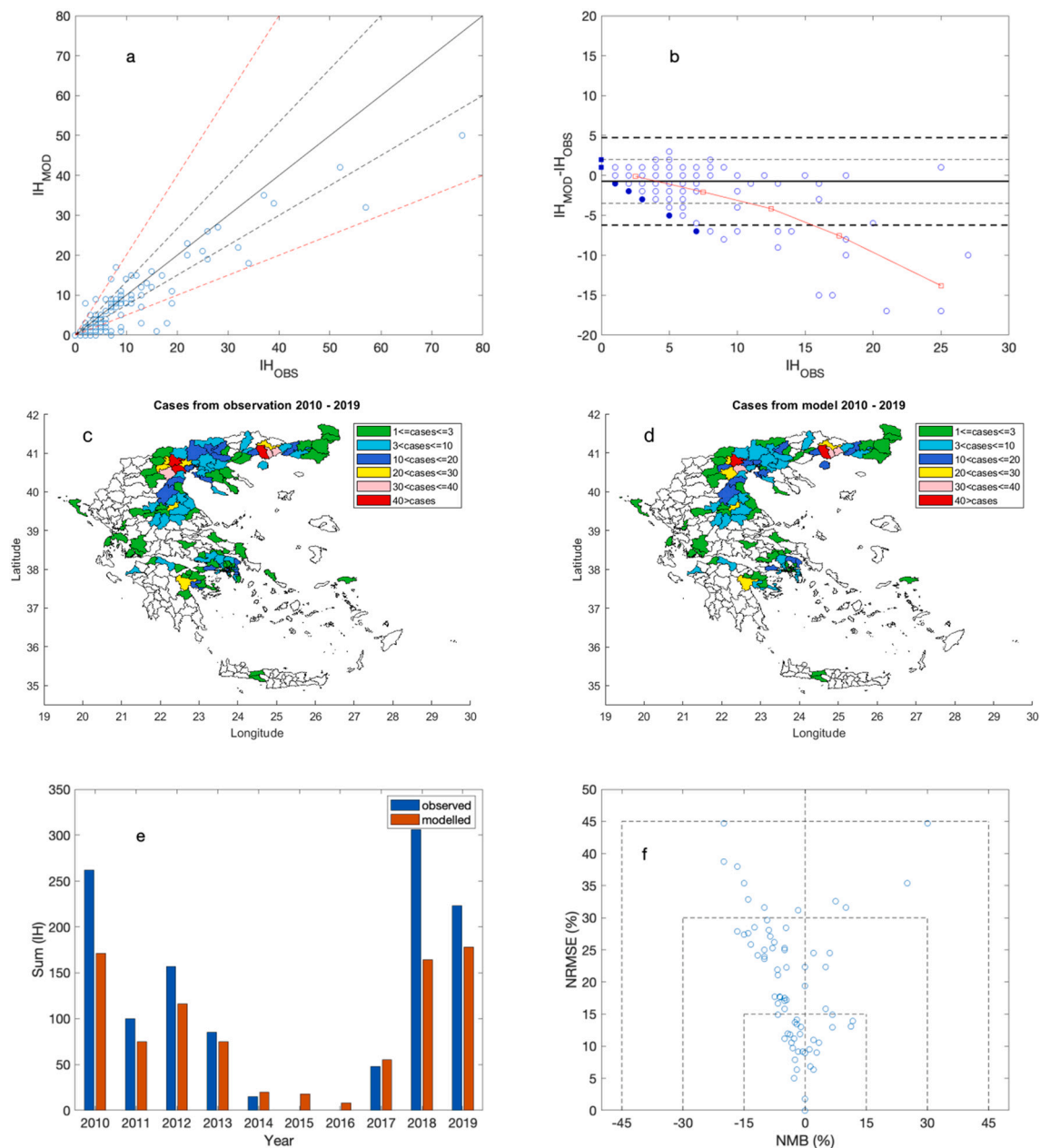
Fig. 4. (a) Observed versus predicted infected human cases at each municipality for the whole decade. The inner line (black) is the main diagonal and the outer lines represent the ±25% (dotted black) and ± 50% (dotted red) bounds around the main diagonal (top left) (b) The residuals (modelled minus observed) versus the observed number of infected humans. The area between the dotted black lines represent the zone [μ-2σ, μ + 2σ]. The binned error is presented with the red line (top right) (c,d) Maps of observed (left) and simulated (right) infected human cases at each municipality for the whole decade (middle row) (e) Temporal evolution of the observed (blue) and predicted (red) annual human cases (bottom left) (f) Soccer diagram for the error (MB, RMSE) at each municipality normalized with the corresponding range of infected humans (bottom right). (For interpretation of the references to colour in this figure legend, the reader is referred to the web version of this article.)

Table 3
The number of observed and modelled infected humans per municipality over the decade decomposed into six zones, with the number of municipalities at each band.

IH	OBS	MOD
1–3	71	56
4–10	47	35
11–20	21	15
21–30	6	5
31–40	4	3
>40	3	2
SUM	**152**	**116**

Table 4
The number of hits, misses and false alarms with respect to the number of infected humans.

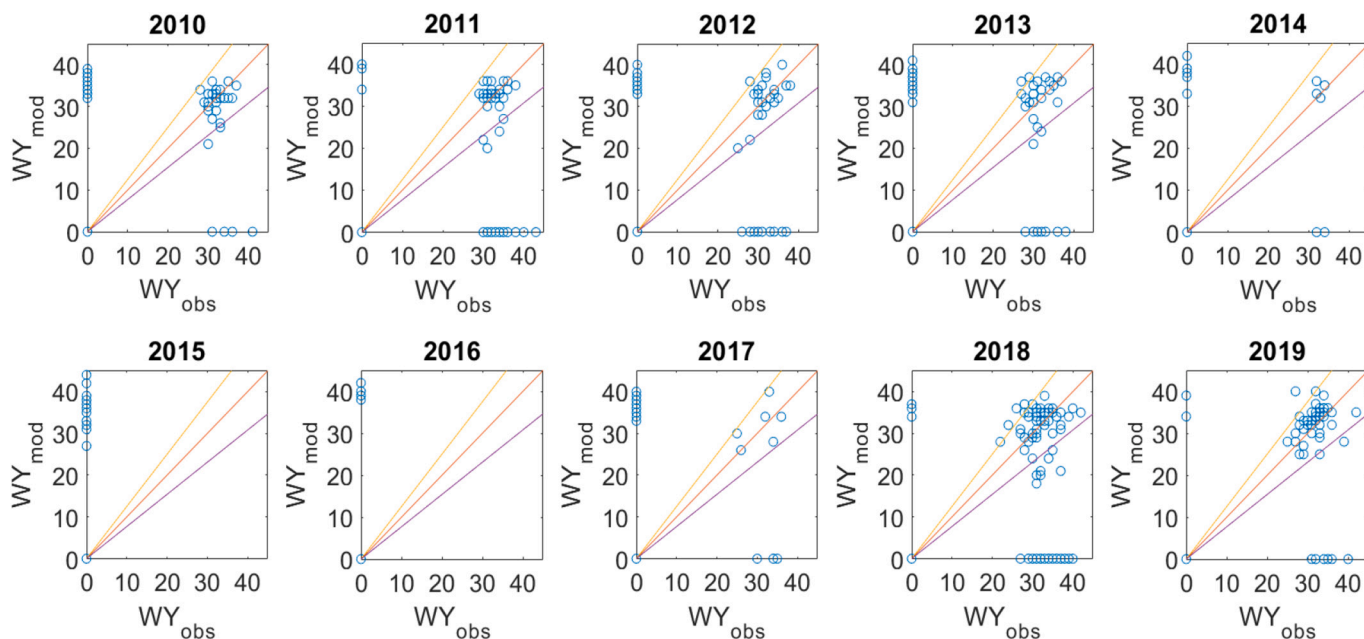| IHobs	a	b	c	a + b + c
1	104	104	72	280
2	35	5	11	51
3	23	–	4	27
≥4	67	–	3	70
SUM	**229**	**109**	**90**	**428**

Fig. 5. Scatter plots of modelled versus observed timing (week) of the 1st human case at each municipality and year. The horizontal axis shows the observed data and the vertical axis presents the modelled data. The red line represents the main diagonal and the other two lines represent the ±25% bounds around the main diagonal. (For interpretation of the references to colour in this figure legend, the reader is referred to the web version of this article.)
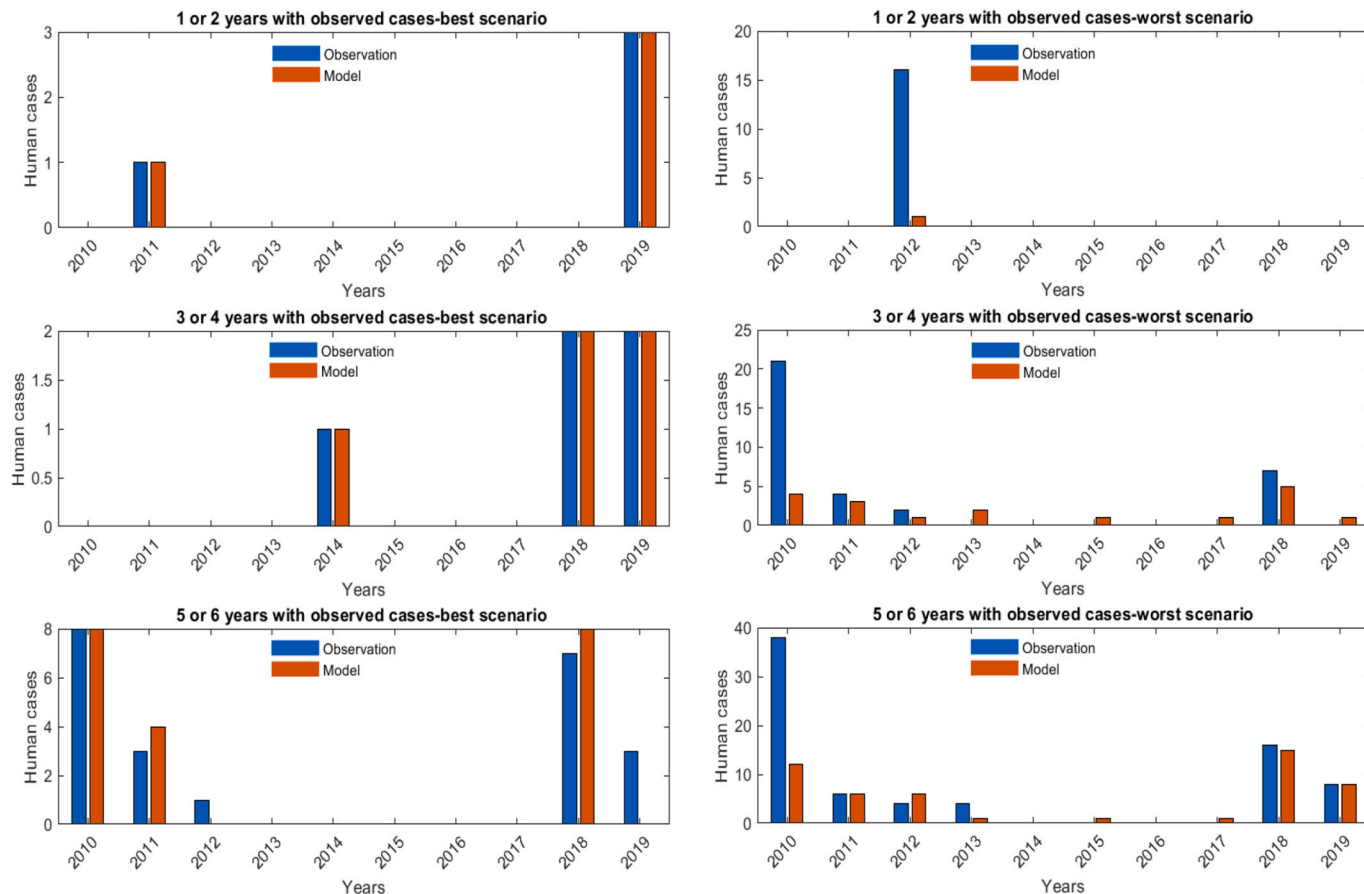

Fig. 6. Demonstration of extreme, with respect to RMSE observed and modelled human cases in municipalities where at least one human case was observed for (a) 1–2 years (top), (b) 3–4 years (middle) and (c) 5–6 years (bottom). Best cases (minimum RMSE) in left column, worst cases (maximum RMSE) in right column.

Table 5

The months whose climatological conditions impact most the severity of the WNV cases, together with the corresponding frequency (number of municipalities), median change in the number of infected humans and median CSI for the group.

#	Combination (months)			Frequency	δIH-50 (%)	CSI-50
1	5			22	33	1
2	6			1	50	0
3	4	5		7	25	1
4	5	6		12	39	1
5	6	7		1	50	1
6	4	5	6	19	33	0.8
7	4	5	8	1	25	0.25
8	5	6	7	30	61	0.75
9	5	6	8	2	71	0.7
10	6	7	8	1	100	1

sensitive to the temperature anomaly in April-May-June (20%) and May-June-July (31%), resulting in a median increase in the total number of cases of 33% and 61% respectively. The corresponding municipalities had a median CSI of 0.8 and 0.75 accordingly.

Common ground at all critical combinations was the month of May, participating either solely or in duet and triplet combination with its neighbor months (4–5, 5–6, 4–5-6, 5–6-7). The median increase in the total infections arising from the 1 °C temperature perturbations generally depended on the participating months but in any case, it exceeded 33%. The median CSI at the most critical combination groups was always larger than 0.75, enhancing the validity of the sensitivity outcome. The importance of the spring temperatures, which shape many mosquito parameters such as breeding and incubation periods, were also found important in other studies (e.g. [62]).

4. Discussion

The aim of this study was to downscale a climate-dependent spatial epidemiological model from the regional level to the municipality level. Purpose of this adaptation was the development of a WNV transmission model for predicting the risk of transmission of WNV to humans considering the climate-sensitivity of pathogen and its vector. In addition, we validated the model using retrospective data. The model (MIMESIS) was applied for the years 2010–2019 in all municipalities of Greece. MIMESIS describes the transmission cycle of the virus between birds, mosquitoes and humans. Model parameters either had constant values, or their values varied with the municipality, the year, the temperature, the precipitation, the daytime length and the Julian day. Two important parameters, the mosquito-human ratio (φ_H) and the initial population of infected mosquitoes ($I_{M,0}$), were optimized during the calibration of the model with the available data. $I_{M,0}$ characterizes the overwintering of the WNV and we assumed it varied spatially and annually; φ_H had only spatial dependence.

MIMESIS successfully discriminated the WNV events at the local (municipal) scale. The probability of detection was 0.72, exceeding 0.80 at 60% of the municipalities, while the false alarm ratio was 0.32, being below 0.20 at over 70% of the municipalities. Similarly, the critical success index and the number of misses were high and low respectively. The critical success index exhibits significant improvement as the number of infected humans and/or the area of the municipality increases. Moreover, the model showed close agreement between observed and predicted number of infected humans at each municipality for the period 2010–2019. The model was unbiased at low incidences (IH < 5), exhibited small underestimation tendency at intermediate cases (5 < IH < 10) and larger underestimation at local outbreaks (IH > 10). The modelled week of emergence of the first human case was scattered around the actual week the incidence appeared, although the distributions were similar. The lack of bias denotes the correct

parameterization curves for the various climate-dependent parameters, such as the mosquito mortality, but at the same time the scatter plot indicates a missing mechanism (e.g. climate-dependent parameterization of transmission probabilities). The interannual variability of WNV dynamics at local scale was well captured. The MIMESIS predicted lower number of infected humans across all years except during the hiatus period 2014–2017, when overestimation occurred.

MIMESIS replicated well the WNV dynamics at 76% of the municipalities where human cases occurred. At the remaining 24% of the municipalities, WNV infections in humans occurred but the model did not predict any. Roughly half of them were limited in densely populated urban areas around the capital city; the other half corresponds to rural or semi-urban municipalities with only one WNV incidence throughout the decade.

To further demonstrate the potential uses of the model, it was also applied in a meteorological sensitivity study, where 1 °C perturbations were introduced to the monthly temperature datasets. Out of the total 298 combinations with temperature variability in one, two or three months, only 10 were critical and the month of May was present in all, pointing the major importance of late spring temperatures in the WNV dynamics.

Our results indicate that the downscaling of a climate-dependent epidemiological model at below NUTS3 spatial scale is doable and one can obtain useful insights. MIMESIS demonstrated skill in the representation of the spatial pattern of WNV emergence, the number of human cases and their timing. The threshold of the downscaling approach was delimited to roughly 80 km². Below this limit, corresponding in our case to densely populated urban sites, the dynamics was beyond the model predictability and the mathematical framework requires additional inputs. Limiting elements in our modelling approach include the assimilation of the rare field entomological data, the issue of population immunity giving rise to 4-year cycles, and of course any sub-grid (i.e. local-scale) process (e.g. stochastic representation of the WNV cycle considering the number of mosquito breeding sites and bird habitats). Moreover, we did not consider in our study the existence, extent and efficiency of possible control strategies to combat larvae and mosquitoes. The next steps include the assimilation of field entomological data, the investigation of the model skill as an early warning tool and the development of a seamless prediction system with meso-scale dynamical models (such as MIMESIS) and local-scale data-driven models.

To the best of our knowledge, this is the first approach to model WNV at this scale over a country and decade.

Climate variability and change affect the spread of vector-borne diseases and the study of the changing transmission dynamics is imperative in efforts to understand them, to forecast outbreaks, to map risks and inform public health authorities. The One Health concept shows and reminds us that human health is linked to animal, environmental and ecosystem health. Therefore, the incorporation of climate and further environmental factors in epidemiological modelling is of major relevance in understanding the transmission of zoonotic diseases such as WNV and in developing appropriate control strategies. The approach can be gradually expanded to incorporate non-environmental factors such as human and animal population movements and change to allow for better prediction of disease risk. Associated data obtained using modern technologies such as earth observation can be used to complement the information derived from classic surveillance of humans, vectors and animals involved in the transmission cycle of vector-borne infectious diseases. Use of new data sources and adaptation of the model allow for the investigation of prevention and response strategies in space and time. The framework of which first elements were presented here has the flexibility and the potential to become a useful tool for early warning and forecasting of vector-borne infectious diseases and contribute to public health decision making.

5. Conclusion

Epidemiological models of mosquito borne diseases such as WNV coupled with climatic factors can be used in improving the forecast capability of the qualitative and quantitative occurrence of infections in time and space. The MIMESIS modelling approach presented here demonstrates that reasonable forecasting potential exist at local scales. Moreover, the model provides an estimate of the time window where cases may occur showing the relevance of seasonal effects of climatic factors such as temperature. The model is a precursor of a broader modelling approach that aspires to capture more human, animal, and environmental aspects to understand the dynamics and control of vector-borne diseases.

Disclaimer

The opinions expressed by the authors do not necessarily reflect the opinions of the European Commission or the institutions with which the authors are affiliated.

Appendix A

The ordinary differential equations (ODES) for mosquitoes, birds and humans are:

$$\frac{dL_M}{dt} = (b_L(T)\delta_M N_M - m_L(T)L_M)\left(1 - \frac{L_M}{K_M}\right) - b_M(T)L_M$$

$$\frac{dS_M}{dt} = -\lambda_{BM}(T)S_M + b_M(T)L_M - m_M(T)S_M$$

$$\frac{dE_M}{dt} = \lambda_{BM}(T)S_M - \gamma_M(T)E_M - m_M(T)E_M$$

$$\frac{dI_M}{dt} = \gamma_M(T)E_M - m_M(T)I_M$$

$$\frac{dS_B}{dt} = \left(b_B - (b_B - m_B)\frac{N_B}{K_B}\right)N_B - \lambda_{MB}(T)S_B - m_B S_B$$

$$\frac{dE_B}{dt} = \lambda_{MB}(T)S_B - \gamma_B E_B - m_B E_B$$

$$\frac{dI_B}{dt} = \gamma_B E_B - \alpha_B I_B - m_B I_B$$

$$\frac{dR_B}{dt} = (1 - \nu_B)\alpha_B I_B - m_B R_B$$

$$\frac{dD_B}{dt} = \nu_B \alpha_B I_B$$

$$\frac{dS_H}{dt} = r_H N_H - \lambda_{MH}(T)S_H$$

$$\frac{dE_H}{dt} = \lambda_{MH}(T)S_H - \gamma_H E_H$$

$$\frac{dI_H}{dt} = \gamma_H E_H - \alpha_H I_H$$

$$\frac{dR_H}{dt} = (1 - \nu_H)\alpha_H I_H$$

$$\frac{dD_B}{dt} = \nu_H \alpha_H I_H$$

where $\lambda_{BM}(T) = \delta_M k(T)p_B\frac{I_B}{K_B}$, $\lambda_{MB}(T) = \delta_M k(T)p_M\varphi_B\frac{I_M}{K_M}$, $\lambda_{MH}(T) = \delta_M k(T)p_M\varphi_H\frac{I_M}{K_M}$.

Appendix B

Parameter	Value	Interpretation	Reference
b_L	$b_L(T) = \dfrac{0.7988}{1 + 1.231 * e^{-0.187(T-20)}}$	Birth rate, larvae	[55]
m_L	$m_L(T) = 0.0025 * T^2 - 0.094 * T + 1.0257$	Mortality rate, larvae	[55]
b_M	$b_M(T) = \dfrac{b_L(T)}{10}$	Birth rate, mosquitoes	[55]
m_M	$m_M(T) = \dfrac{m_L(T)}{10}$	Mortality rate, mosquitoes	[55]
γ_M	$\gamma_M(T) = 0.0093 * T - 0.1352, T > 15^\circ C$ $\gamma_M(T) = 0, T \le 15^\circ C$	Rate with $1/\gamma_M$ extrinsic-incubation period	[55]
δ_M	$\delta_M(D) = 1 - \dfrac{1}{1 + 1775.7 * e^{1.559(D-18.177)}}$	Fraction mosquitoes non- diapausing	[55]
k	$k(T) = \dfrac{0.344}{1 + 1.231 * e^{0.184(T-20)}}$	Mosquito biting rate	[55]
b_B	$b_B(d) = \dfrac{\left(\dfrac{d}{\beta}\right)^{\alpha-1} * e^{-\frac{d}{\beta}}}{\beta\Gamma(\alpha)}$	Birth rate, birds	[55]
p_M	0.90	WN transmission probability (mosquito to bird)	[42]
m_B	0.00034	Mortality rate, birds	[54]
p_B	0.125	WN transmission probability (bird to mosquito)	[42,54]

(continued)

α_B	0.4	Removal rate, birds	[54]
γ_B	1.0	Rate with $1/\gamma_B$ intrinsic incubation period	[54]
ν_B	0.7	Fraction birds dying due to infection	[54]
φ_B	30	Mosquito to bird ratio	[54]
b_H	0.000033	Birth rate, humans	[57]
m_H	0.000034	Mortality rate, humans	[57]
r_H	$r_H = b_H - m_H$	Reproduction rate, humans	[57]
α_H	0.5	Removal rate, humans	[54]
γ_H	0.25	Transition rate from exposed to infected, humans	[54]
ν_H	0.004	Fraction humans dying due to infection	[54]
φ_H	φ_H (municipality)	Mosquito to human ratio	After calibration
$I_{M,0}$	$I_{M,0}$ (municipality, year)	Infectious mosquitoes	After calibration
$N_{M,min}$	$N_{M,min}$ (municipality)	Susceptible mosquitoes	[54] [57]
K_B	K_B (municipality)	Carrying capacity, birds	[58]
K_M	K_M(municipality, R_{CUM}) = K_B (municipality) * φ_B * (0.75 + 0.25 * R_{CUM})	Carrying capacity, mosquitoes	[56]
$N_{H,0}$	$N_{H,0}$ (municipality)	Susceptible humans	[57]

Parameter definition of the WNV model. In the formulas, T is the air temperature, D is daytime length in hours, d is the Julian day of the year, Γ is the Gamma distribution with $\alpha = 86.4$ and $\beta = 1.4$ and R_{CUM} is the accumulated precipitation over the previous two weeks, normalized in [0,1] by dividing with the maximum value reached throughout the year. The subscript 0 denotes initial condition.

Appendix C

Abbreviation	Description
WNV	West Nile Virus
WNF	West Nile Fever
WNND	West Nile neuro-invasive disease
MIMESIS	spatial dynaMIcal Model for wESt nIle viruS
HCDCP	Hellenic Center for Disease Control and Prevention
EBBA	European Breeding Birds Atlas
EBCC	European Bird Census Board
ECMWF	European Centre for Medium Weather Forecast
L_M	Larvae Mosquitoes
S_M	Susceptible Mosquitoes
E_M	Exposed Mosquitoes
I_M	Infectious Mosquitoes
S_B	Susceptible Birds
E_B	Exposed Birds
I_B	Infectious Birds
R_B	Recovered Birds
D_B	Dead Birds
S_H	Susceptible Humans
E_H	Exposed Humans
I_H	Infectious Humans
R_H	Recovered Humans
D_H	Dead Humans
RMSE	Root-Sean-Square Error
POD	Probability of Detection
MIS	Miss Rate
FAR	False-alarm rate
CSI	Critical Success Index
MB	Mean Bias
IH	Infected Humans (annual aggregation at each municipality)
IH_{MOD}	Modelled IH
IH_{OBS}	Observed IH
SD	Standard Deviation
NMB	Normalized Mean Bias
NRMSE	Normalized Root-Sean-Square Error

Appendix D. Supplementary data

Supplementary data to this article can be found online at https://doi.org/10.1016/j.onehlt.2021.100330.

References

[1] World Health Organization, Vector-borne diseases, Available online: https://www.who.int/news-room/fact-sheets/detail/vector-borne-diseases, 2021 (accessed September 2021).

[2] World Health Organization, Climate Change and Human Health - Risks and Responses. Summary, WHO, 2003. ISBN 9241590815.

[3] K.D. Lafferty, The ecology of climate change and infectious diseases, Ecology 90 (2009) 888–900, https://doi.org/10.1890/08-0079.1.

[4] T.M. Colpitts, M.J. Conway, R.R. Montgomery, E. Fikrig, West Nile Virus: biology, transmission, and human infection, Clin. Microbiol. Rev. 25 (2012) 635–648, https://doi.org/10.1128/CMR.00045-12.

[5] K.C. Smithburn, T.P. Hughes, A.W. Burke, J.H. Paul, A neurotropic virus isolated from the blood of a native of Uganda, Am. J. Trop. Med. Hyg. S1-S20 (1940) 471–492.

[6] L. Bertolotti, U.D. Kitron, E.D. Walker, M.O. Ruiz, J.D. Brawn, S.R. Loss, G.L. Hamer, T.L. Goldberg, Fine-scale genetic variation and evolution of West Nile

Virus in a transmission "hot spot" in suburban Chicago, USA, Virology 374 (2008) 381–389, https://doi.org/10.1016/j.virol.2007.12.040.

[7] Z. Hubalek, J. Halouska, West Nile fever - A reemerging mosquito-borne viral disease in Europe, Emerg. Infect. Dis. 5 (1999) 643–650, https://doi.org/10.3201/eid0505.990505.

[8] T.J. Gray, C.E. Webb, A review of the epidemiological and clinical aspects of West Nile virus, Int. J. Gen. Med. 7 (2014) 193–203, https://doi.org/10.2147/IJGM.S59902.

[9] G. Marini, P. Poletti, M. Giacobini, A. Pugliese, S. Merler, R. Rosà, The role of Climatic and density dependent factors in shaping mosquito population dynamics: the case of culex pipiens in Northwestern Italy, PLoS One 11 (4) (2016), e0154018, https://doi.org/10.1371/journal.pone.0154018.

[10] G. Valiakos, A. Touloudi, C. Iacovakis, L. Athanasiou, P. Birtsas, V. Spyrou, C. Billinis, Molecular detection and phylogenetic analysis of West Nile virus lineage 2 in sedentary wild birds (Eurasian magpie), Greece, 2010, Euro Surveill. 16 (2011).

[11] World Health Organization, West Nile Virus, Available online: https://www.who.int/en/news-room/fact-sheets/detail/west-nile-virus (accessed on April 2020).

[12] A. Papa, West Nile virus infections in humans — Focus on Greece, J. Clin. Virol. 58 (2013) 351–353, https://doi.org/10.1016/j.jcv.2013.02.020.

[13] A. Maxmen, The hidden threat of West Nile virus, Nature 489 (2012) 349–350, https://doi.org/10.1038/489349a.

[14] Hellenic Center for Disease Control and Prevention (HCDCP), Report on West Nile Virus Epidemic. http://www.keelpno.gr/, 2018.

[15] S. Paz, J.C. Semenza, Environmental drivers of West Nile Fever epidemiology in Europe and Western Asia–A review, Int. J. Environ. Res. Public Health 10 (2013) 3543–3562, https://doi.org/10.3390/ijerph10083543. PMID: 23939389.

[16] S. Paz, Climate change impacts on West Nile virus transmission in a global context, Philos. Trans. R. Soc. B: Biol. Sci. 370 (2015) 20130561, https://doi.org/10.1098/rstb.2013.0561.

[17] C.B.F. Vogels, N. Hartemink, C.J.M. Koenraadt, Modelling West Nile virus transmission risk in Europe: effect of temperature and mosquito biotypes on the basic reproduction number, Sci. Rep. 7 (2017) 5022, https://doi.org/10.1038/s41598-017-05185-4.

[18] B.V. Giordano, S. Kaur, F.F. Hunter, West Nile virus in Ontario, Canada: a twelve year analysis of human case prevalence, mosquito surveillance, and climate data, PLoS One 12 (2017), e0183568.

[19] N.I. Stilianakis, V. Syrris, Th. Petroliagkis, P. Part, S. Gewehr, S. Kalaitzopoulou, S. Mourelatos, A. Baka, D. Pervanidou, J. Vontas, C. Hadjichistodoulou, Identification of climatic factors affecting the epidemiology of human West Nile Virus infections in northern Greece, PLoS One 11 (9) (2016), e0161510.

[20] W.M. Chung, C.M. Buseman, S.N. Joyner, S.M. Hughes, T.B. Formby, J.P. Luby, et al., The 2012 West Nile encephalitis epidemic in Dallas Texas, JAMA 310 (2013) 297–307, https://doi.org/10.1001/jama.2013.8267. PMID: 23860988.

[21] M.C. Wimberly, A. Lamsal, P.C. Giacomo, T.W. Chuang, Regional variation of climatic influences on West Nile Virus outbreaks in the United States, Am. J. Trop. Med. Hyg. 91 (2014) 677–684, https://doi.org/10.4269/ajtmh.14-0239. PMID: 25092814.

[22] X. Liu, Baimaciwang, Y. Yue, H. Wu, Pengcuociren, Y. Guo, D. Ren Cirenwangla, Dazhlen Dancenggongba, J. Yang, Zhaxisangmu, J. Li, Cirendeji, N. Zhao, J. Sun, J. Wang Cirendunzhu Li, Q. Liu, Breeding site characteristics and associated factors of Culex pipiens complex in Lhasa, Tibet, P.R. China, Int. J. Environ. Res. Public Health 16 (2019) 1407.

[23] W.E. Britton, A remarkable outbreak of Culex pipiens Linn, J. Econ. Entomol. 7 (1914) 257–260.

[24] T. Takeda, C.A. Whitehouse, M. Brewer, A.D. Gettman, T.N. Mather, Arbovirus surveillance in Rhode Island: assessing potential ecologic and climatic correlates, J. Am. Mosq. Control Assoc. 19 (2003) 179–189.

[25] L.M. Calhoun, M. Avery, L. Jones, K. Gunarto, R. King, J. Roberts, T.R. Burkot, Combined sewage overflows (CSO) are major urban breeding sites for Culex quinquefasciatus in Atlanta, Georgia, Am. J. Trop. Med. Hyg. 77 (2007) 478–484, https://doi.org/10.4269/ajtmh.2007.77.478.

[26] J.E. Soverow, G.A. Wellenius, D.N. Fisman, M.A. Mittleman, Infectious disease in a warming world: how weather influenced West Nile virus in the United States (2001–2005), Environ. Health Perspect. 117 (2009) 1049–1052, https://doi.org/10.1289/ehp.0800487.

[27] C.J.M. Koenraadt, L. Harrington, Flushing effect of rain on container-inhabiting mosquitoes Aedes aegypti and Culex pipiens (Diptera: Culicidae), J. Med. Entomol. 45 (2008) 28–35, https://doi.org/10.1603/0022-2585(2008)45[28:feoroc]2.0.co;2.

[28] J. Shaman, M. Stieglitz, C. Stark, S. Le Blancq, M. Cane, Using a dynamic hydrology model to predict mosquito abundances in flood and swamp water, Emerg. Infect. Dis. 8 (2002) 6–13, https://doi.org/10.3201/eid0801.010049.

[29] D.J. Dohm, M.L. O'Guinn, M.J. Turell, Effect of environmental temperature on the ability of Culex pipiens (Diptera: Culicidae) to Transmit West Nile Virus, J. Med. Entomol. 39 (2002) 221–225, https://doi.org/10.1603/0022-2585-39.1.221.

[30] W.K. Reisen, Y. Fang, V.M. Martinez, Effects of temperature on the transmission of West Nile virus Culex tarsalis (Diptera: Culicidae), J. Med. Entomol. 43 (2006) 309–317, https://doi.org/10.1603/0022-2585(2006)043[0309:EOTOTT]2.0.CO;2.

[31] L. Rueda, K. Patel, R. Axtell, R. Stinner, Temperature-dependent development and survival rates of Culex quinquefasciatus and Aedes aegypti (Diptera: Culicidae), J. Med. Entomol. 27 (1990) 892–898, https://doi.org/10.1093/jmedent/27.5.892.

[32] C.G. Smith, Factors influencing the transmission of western equine encephalomyelitis virus between its vertebrate maintenance hosts and from them

to humans, Am. J. Trop. Med. Hyg. 37 (1987) 33S–39S, https://doi.org/10.4269/ajtmh.1987.37.33S.

[33] J.M. Chase, T.M. Knight, Drought-induced mosquito outbreaks in wetlands, Ecol. Lett. 6 (2003) 1017–1024, https://doi.org/10.1046/j.1461-0248.2003.00533.x.

[34] Y. Vardanis, R.H. Klaassen, R. Strandberg, T. Alerstam, Individuality in bird migration: routes and timing, Biol. Lett. 7 (2011) 502–505, https://doi.org/10.1098/rsbl.2010.1180.

[35] T.F. Tsai, F. Popovici, C. Cernescu, G.L. Campbell, N.I. Nedelcu, West Nile encephalitis epidemic in southeastern Romania, Lancet 352 (1998) 767–771, https://doi.org/10.1016/S0140-6736(98)03538-7.

[36] R.S. Lanciotti, J.T. Roehrig, V. Deubel, J. Smith, M. Parker, K. Steele, et al., Origin of the West Nile virus responsible for an outbreak of encephalitis in the northeastern United States, Science 286 (1999) 2333–2337, https://doi.org/10.1126/science.286.5448.2333.

[37] S. Napp, D. Petric, N. Busquets, West Nile virus and other mosquito-borne viruses present in Eastern Europe, Pathog. Glob. Health 112 (2018) 233–248, https://doi.org/10.1080/20477724.2018.1483567.

[38] European Centre for Prevention and Control (ECDC), Epidemiological Update West Nile Virus Transmission Season in Europe. https://www.ecdc.europa.eu/en/publications-data/west-nile-virus-infection-annual-epidemiological-report-2018, 2019.

[39] E. Parselia, C. Kontoes, A. Tsouni, C. Hadjichristodoulou, I. Kioutsioukis, G. Magiorkinis, N.I. Stilianakis, Satellite earth observation data in epidemiological modeling of malaria, dengue and west nile virus: a scoping review, Remote Sens. 11 (2019) 1862, https://doi.org/10.3390/rs11161862.

[40] C. Barker, Models and surveillance systems to detect and predict West Nile virus outbreaks, J. Med. Entomol. 56 (2019) 1508–1515, https://doi.org/10.1093/jme/tjz150.

[41] D.M. Thomas, B. Urena, A model describing the evolution of West Nile-like encephalitis in New York City, Math. Comput. Model. 34 (2001) 771–781, https://doi.org/10.1016/S0895-7177(01)00098-X.

[42] M.J. Wonham, T. de Camino Beck, M.A. Lewis, An epidemiological model for West Nile virus: invasion analysis and control applications, Proc. R. Soc. Series B: Biol. Sci. 27 (1538) (2004) 501–507.

[43] M. Lewis, J. Renčlawowicz, P.V. den Driessche, Traveling waves and spread rates for a West Nile virus model, Bull. Math. Biol. 68 (1) (2006) 3–23.

[44] J. Jiang, Z. Qiu, J. Wu, H. Zhu, Threshold conditions for West Nile virus outbreaks, Bull. Math. Biol. 71 (3) (2009) 627–647.

[45] G. Fan, J. Liu, P. van den Driessche, J. Wu, H. Zhu, The impact of maturation delay of mosquitoes on the transmission of West Nile virus, Math. Biosci. 228 (2) (2010) 119–126.

[46] Z. Lin, H. Zhu, Spatial spreading model and dynamics of West Nile virus in birds and mosquitoes with free boundary, J. Math. Biol. 75 (6–7) (2017) 1381–1409.

[47] J. Zhang, C. Cosner, H. Zhu, Two-patch model for the spread of West Nile virus, Bull. Math. Biol. 80 (4) (2018) 840–863.

[48] G. Cruz-Pacheco, L. Esteva, C. Vargas, Seasonality and outbreaks in West Nile virus infection, Bull. Math. Biol. 71 (6) (2009) 1378–1393.

[49] D.M. Hartley, W.K. Reisen, T. Niu, H.D. Gaff, C.M. Barker, A. Le Menach, Effects of temperature on emergence and seasonality of West Nile virus in California, Am. J. Trop. Med. Hyg. 86 (5) (2012) 884–894.

[50] P. Moschini, D. Bisanzio, A. Pugliese, A seasonal model for West Nile virus, Math. Model. Natur. Phenomena 12 (2) (2017) 58–83.

[51] N.B. DeFelice, Z.D. Schneider, E. Little, C. Barker, L.A. Cailouet, S.R. Campbell, D. Damian, P. Irwin, H.M.P. Jones, J. Townsend, J. Shaman, Use of temperature to improve West Nile virus forecasts, PLoS Comput. Biol. 14 (3) (2018), e1006047.

[52] G. Marini, R. Rosa, A. Pugliese, A. Rizzoli, C. Rizzo, F. Russo, F. Montarsi, G. Capelli, West Nile Virus transmission and human infection risk in Veneto (Italy): a modelling analysis, Sci. Rep. 8 (2018) 14005.

[53] D. Montecino-Latorre, C.M. Barker, Overwintering of West Nile virus in a bird community with a communal crow roost, Sci. Rep. 8 (2018) 6088.

[54] V. Laperriere, K. Brugger, F. Rubel, Simulation of seasonal cycles of bird, equine and human West Nile virus cases, Prev. Vet. Med. 98 (2011) 99–110, https://doi.org/10.1016/j.prevetmed.2010.10.013.

[55] F. Rubel, K. Brugger, M. Hantel, S. Chvala, T. Bakonyi, H. Wessenböck, N. Nowotny, Explaining Usutu virus dynamics in Austria: model development and calibration, Prev. Vet. Med. 85 (2008) 166–186, https://doi.org/10.1016/j.prevetmed.2008.01.006.

[56] I. Kioutsioukis, N.I. Stilianakis, Assessment of West Nile virus transmission risk from a weather-dependent epidemiological model and a global sensitivity analysis framework, Acta Trop. 193 (2019) 129–141, https://doi.org/10.1016/j.actatropica.2019.03.003.

[57] Hellenic Statistical Authority (HSA). https://www.statistics.gr/en/home/, 2011.

[58] European Bird Census Council (EBCC). https://www.ebba2.info/ebba1/, 2021.

[59] C. Hadjichristodoulou, S. Pournaras, M. Mavrouli, A. Marka, P. Tserkezou, A. Baka, et al., West Nile Virus Seroprevalence in the Greek population in 2013: a nationwide cross-sectional survey, PLoS One 10 (11) (2015), e0143803, https://doi.org/10.1371/journal.pone.0143803.

[60] Y. Wang, W. Pons, J. Fang, H. Zhu, The impact of weather and storm water management ponds on the transmission of West Nile virus, R. Soc. Open Sci. 4 (2017), 170017, https://doi.org/10.1098/rsos.170017.

[61] I.G. Zurbenko, The Spectral Analysis of Time Series, 1986, p. 236. North-Holland, Amsterdam.

[62] G. Marini, M. Calzolari, P. Angelini, R. Bellini, S. Bellini, L. Bolzon, et al., A quantitative comparison of West Nile virus incidence from 2013 to 2018 in Emilia-Romagna, Italy, PLoS Negl. Trop. Dis. 14 (1) (2020), e0007953, https://doi.org/10.1371/journal.pntd.0007953.